

Detection of shallow inclusions in closed-packed granular beds using mechanical impulses

Saravanan Swaminathan, Donald P. Visco, Jr

Department of Chemical Engineering, Tennessee Technological University, Cookeville,
Tennessee 38505

Surajit Sen*

Physics Department, State University of New York, Buffalo, New York 14260

Abstract

Mechanical energy has been used in the detection of shallow buried objects in granular beds for more than half a century. Here we attempt to answer a fundamental question – *at what depths would an object be detectable in an idealized, close packed, granular bed made of monosized elastic spheres?* Systematic particle dynamics based studies reveal the effects of varying the area across which the impulse is generated, object size and restitution on locating the buried object.

PACS Nos: 81.05.Rm,83.80.Fg,45.70.-n,05.45.-a,07.05.Tp

*Corresponding author: sen@nsm.buffalo.edu

The problem of acoustically detecting *shallow*, buried objects in granular beds has a rich history [1-8]. There are even accounts from the life sciences about how doodlebugs or antlions survive in the soil using sound waves [9]. Much of the work has been done by those involved in acoustic landmine detection and are largely experimental and records of conference presentations [1,10] and often without reference to studies from the academic communities. As a result, well known issues such as the inadequacy of the wave equation to describe mechanical energy propagation [11] through shallow soil have been often ignored in much of the existing literature [1,2,8,10].

There are a few experimental studies of impulse propagation at shallow depths of granular beds [7,8,12]. These demonstrate that energy propagation is sensitive to packing and is not like wave propagation by revealing that the signal speed depends upon amplitude and that signal dispersion is limited [12]. Here we address a fundamental question - *at what depths would an object be detectable in an idealized, close packed, granular bed made of monosized elastic spheres?* To answer this question, one must consider the velocity perturbation imparted to the surface grains, the perturbation area, obstacle size, obstacle depth, the nature of granular contacts and the amount of restitutional loss [13].

We consider the propagation of a velocity perturbation imparted onto a fixed area A ($\equiv L \times L$), measured in grain diameters, as shown in Figure 1(a). Detection of shallow objects, which are likely to produce significant backscattering is a challenge. To study this, we create a system comprised of $40 \times 40 \times 60$ monodisperse quartz spheres of radius R grains in a hexagonal-close-packed (hcp) lattice [13]. The spheres interact upon compression via the nonlinear Hertz potential [14], $V(\delta_{ij}) = a\delta_{ij}^{5/2}$, where $a = (2/5D)(R/2)^{1/2}$, $R = 0.5 \times 10^{-4}$ m, $D \equiv 3(1 - \sigma^2)/2Y$, $Y = \text{Young's modulus } (7.87 \times 10^{10} \text{ Nm}^{-2})$, $\sigma = 0.144$ is the Poisson's ratio for

quartz and the grain overlap parameter $\delta_{ij} \equiv 2R - (|\vec{r}_i - \vec{r}_j|) \geq 0$, where (i, j) are neighbors in contact in the hcp lattice. Such a potential is steeper than harmonic at large enough compressions but is softer than harmonic at small compressions. This potential, along with the requirement of momentum conservation, leads to effectively ballistic-like energy transport [12,13].

We set the velocity of all the grains to be zero at $t = 0$ except for those centered on an area A at the bed surface. All subsequent grain positions, velocities and accelerations are computed by numerically integrating the equation of motion for each grain via the Velocity-Verlet algorithm [15] using a 0.1 μsec timestep of integration. A larger timestep introduces errors and a smaller timestep does not yield significant benefits. The perturbation propagates as a compression pulse into the system. The effect of restitution (e) is included via the inter-grain force during loading and unloading [16], $F_{unload} / F_{load} \equiv 1 - e$, where $0 < e < 1$ defines the restitution parameter with F_{load} (F_{unload}) referring to the (de)compression force between two grains in contact. Hence, $e = 0(1)$ denotes completely (in)elastic behavior. To avoid wall reflection effects, the four side-walls and the bottom wall are made completely *energy absorptive*. To study a range of impulse areas, we use $L = 2, 4, 6, 8, 10, 12, 14, 16, 18$ and 20 (in grain diameters) while using a variety of obstacle areas OA ($\equiv OL \times OL$) where $OL = 2, 4, 6, 8$ and 10. Additionally, to explore the effects of restitution, we let $e = 0$ and 0.04 (4% restitution).

The impulse is initiated across an area of the surface. The energy spreads in a cone-shaped-form as sketched in Figure 1(a). Impulse velocities of 5m/s and 50m/s were used to study the cumulative backscattering at the second layer. It was found that for the case of 5m/s, the backscattering was too weak to be easily detected and, thus, we decided to use an impulse velocity of 50m/s. In this work, we examine the time integrated or cumulative kinetic energy at the surface. We define the cumulative average kinetic energy per surface grain

$\kappa(t) \equiv \sum_0^t (1/N_s) \sum_{N_s} p_i^2(\tau) / 2m$, where N_s is the number of surface grains, τ is a dummy

variable for time and $\kappa(t)$ is averaged over all time from $\tau = 0$ to $\tau = t$. Figure 1(b) illustrates the dynamic behavior of $\kappa(t)$ for a few representative impulse areas. Note that κ reaches a quick *minimum* as the energy enters into the bed and then grows in time to reach an asymptotic value, κ_{final} . Figure 1(b) confirms $\kappa_{final} L = \text{constant}$ [13]. The larger the L , the less is the energy backscattered to the surface. Further, introducing restitution reduces the magnitude of κ_{final} .

Having characterized the dynamics of the empty bed, we introduce the object to be detected. Here we examine all combinations of object size ($OL = 2, 4, 6, 8$ and 10), object location (Layer depth = $4, 6, 8, 10, 12, 14, 16, 18, 20, 25$ and 30) and impulse area ($L = 2, 4, 6, 8, 10, 12, 14, 16, 18$ and 20). Since we are interested in the effect of the presence of the obstacle on backscattered energies, we calculate a κ_{diff_final} ($\equiv \kappa_{final\ bed\ (with\ obstacle)} - \kappa_{final\ (without\ obstacle)}$), which is the difference in κ_{final} between the pure bed and that with the obstacle. The κ_{diff_final} values for *all* cases can be found elsewhere [17].

Ultimately, we determine if the object is detectable by analyzing the values of κ_{diff_final} . If $\kappa_{diff_final} < 0$, it is an indication that the impulse area is smaller than the obstacle area resulting in a reduction of the number of particles participating in the backscattering. Here, many layers of grains directly beneath the object are effectively shielded from the impulse. If $\kappa_{diff_final} > 0$, it indicates that the backscattering from the buried object exceeds the ambient backscattering present from the empty bed. Figure 2 illustrates the profile of κ_{diff_final} when placing the obstacle at two representative layers. It can be seen in Figure 2(a) that there is a peak for every obstacle area near the value of the impulse area. This indicates that at shallow depths (Layer = 4), we get

maximum backscattering for the cases when $L \geq OL$. The other key feature that can be seen in Figure 2(a) is that κ_{diff_final} values cross-over from the negative to the positive region when the $L \approx OL$. Figure 2(b) depicts the trend of κ_{diff_final} values when the obstacles are placed in the 20th layer. It can be seen that the peak in this case occurs when $L > OL$. This is due to the fact that as the obstacle depth is increased, there is attenuation in the magnitude of the κ_{diff_final} which, in turn, leads requiring larger impulse areas to detect the presence of smaller obstacles.

To form an overall picture of the ability to detect the smallest object using different impulse areas, larger scale dynamical studies are warranted. However, global ‘phase diagrams’ for small systems can be constructed, as in Figure 3, by performing many simulations using various impulse areas and obstacle lengths. As there are sensors that can detect energies of 0.2pJ [18], these diagrams have been constructed for two reasonable energy “resolutions,” 10nJ and 100nJ (where “resolution” defines the smallest detectable energy) for the values of κ_{diff_final} at long enough times (i.e. 2×10^4 timesteps). The results in Figure 3 are for $e = 0$. The different regions shown with different shades indicate the detectability of the different obstacle areas using representative impulse areas. Note that negative values of κ_{diff_final} can be detected (if greater than the resolution) since this value is not a negative absolute energy, but relative to that of the empty bed. In each of these cases, the values of κ_{diff_final} depend on whether or not restitutional losses are present. We find that as the resolution increases, there is significant change in the phase diagram for a selected impulse area. Comparing all the cases in Figure 3, it can be seen that the shape of phase diagrams is insensitive to changes in the resolution and the restitution.

We have studied the detectability of small buried objects at shallow depths using backscattering of different mechanical impulse across small areas. The results are shown by

constructing global “phase diagrams.” Our study suggests that there exists a relationship between the size of the impulse area and the size of the obstacle area, a result that may be vital for detectability of small buried objects at shallow depths.

We thank ARO and NSF for partial support.

References:

- [1] There are several reports on buried object detection that are not refereed contributions but are available, e.g., J.F. Mifsud, Report DRL-A-95 (October 1955); S. Rickser, Report DRL-A-98 (December 1955); D.A. Sachs, B.G. Watters, P.K. Krumhansel, P.W. Smith, J. Doherty, J. Webb, and A. Davidson, BBN Technical Report No. 7677 (3 volumes), submitted to the U.S. Army Belvoir Research and Development Center, 1992.
- [2] J.C. Cook and J.J. Wormser, IEEE Trans on Geoscience Electronics, **GE11**, 135 (1973).
- [3] A. Shukla and C. Damania, J. Exper. Mech. **27**, 268 (1987).
- [4] C.Y. Zhu, A. Shukla and M.H. Sadd, J. Appl. Mech. **58**, 341 (1991).
- [5] A.J. Rogers and C.G. Don, Acoustics Australia **22**, 5 (1994).
- [6] R.S. Sinkovits and S. Sen, Phys. Rev. Lett. **74**, 2686 (1995).
- [7] A. Britan, G. Ben-Dor, T. Elperin, O. Igra and J.P. Jiang, Exper. Fluids **22**, 432 (1997).
- [8] G.S. Baker, C. Schmeissner, D.W. Steeples and R.G. Plumb, Geophys. Res. Lett. **26**, 279 (1999).
- [9] J.T. Botz, C. Loudon, J.B. Barger, J.S. Olafsen and D.W. Steeples, Integrative and Compar. Biol. **42**, 6 (2002).
- [10] There are several SPIE Conf Proceedings with reports on work on acoustic land mine detection, see for example, A. Dubey, J. Harvey, J.T. Broach and V. George, Proc of SPIE, **4394** (SPIE, Bellingham, 2001).
- [11] S. Sen, T.R. Krishna Mohan, D.P. Visco, Jr., S. Swaminathan, A. Sokolow, E. Avalos and M. Nakagawa, Int. J. of Mod. Phys. B **19**, 2951 (2005) and references therein.
- [12] S.R. Hostler and C.E. Brennen, Phys. Rev. E **72**, 031303 (2005); *ibid* **72**, 031304 (2005).

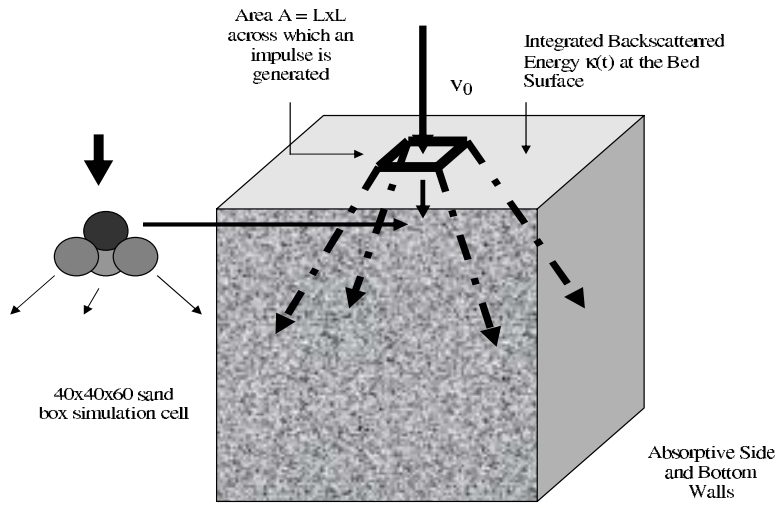
- [13] D.P. Visco, Jr., S. Swaminathan, T.R. Krishna Mohan, A. Sokolow and S. Sen, Phys. Rev. E **70**, 051306 (2004).
- [14] H. Hertz, J. reine u. Angew. Math. **92**, 156 (1881).
- [15] M.P. Allen and D.J. Tildesley, Computer Simulation of Liquids (Clarendon, Oxford, 1987).
- [16] O.R. Walton and R.L. Braun, J. Rheol. **30**, 949 (1986).
- [17] http://electron.physics.buffalo.edu/~sen/documents/apl_don_SupplementalMaterial.pdf
- [18] <http://www.coherentinc.com/Lasers/index.cfm?fuseaction=show.page&id=961> (as on 16th January, 2007)

Figure Captions:

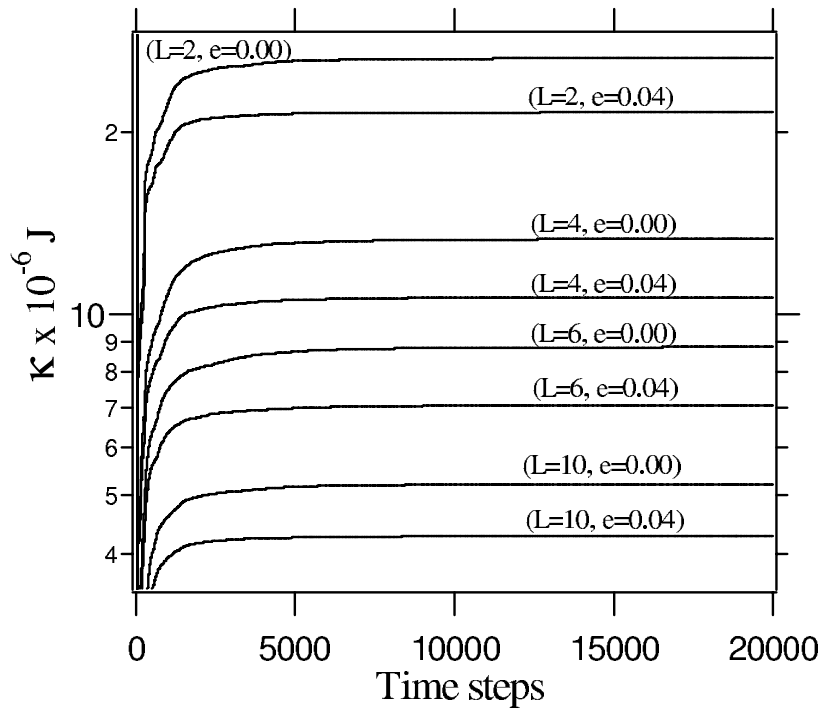
Figure 1. (a) Schematic diagram of the system (b) Effect of restitution (e) on κ for different impulse areas (L). Note that no obstacle is present in the bed.

Figure 2. (a) κ_{diff_final} vs. Impulse area for five different obstacle areas ($OL = 2, 4, 6, 8$ and 10) at layer 4. (b) κ_{diff_final} vs. Impulse area for five different obstacle areas ($OL = 2, 4, 6, 8$ and 10) at layer 10.

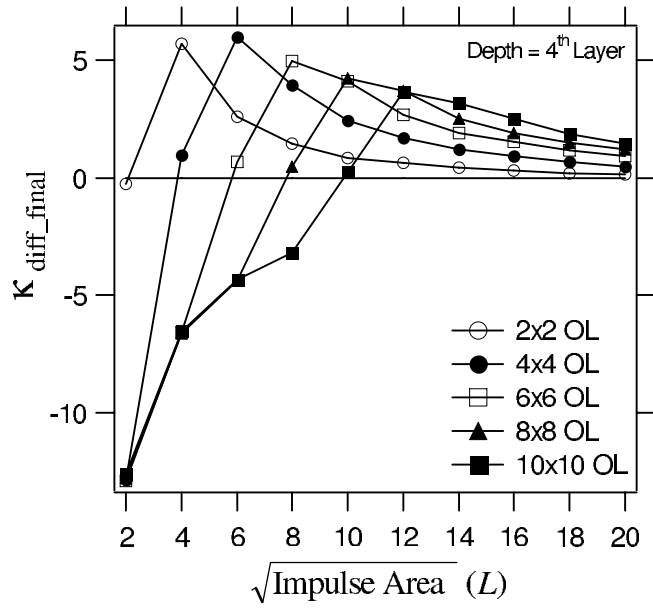
Figure 3. (a) Global phase diagram without restitution for a resolution of $10nJ$. (b) Global phase diagram without restitution for a resolution of $100nJ$.



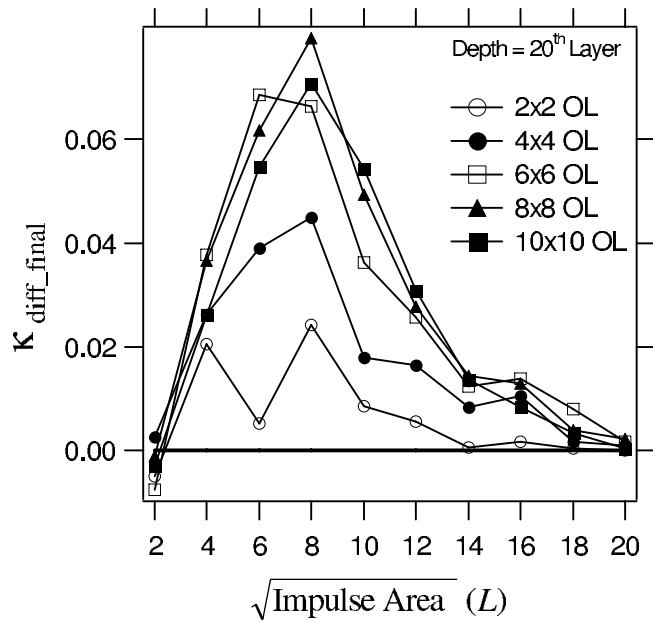
(a)



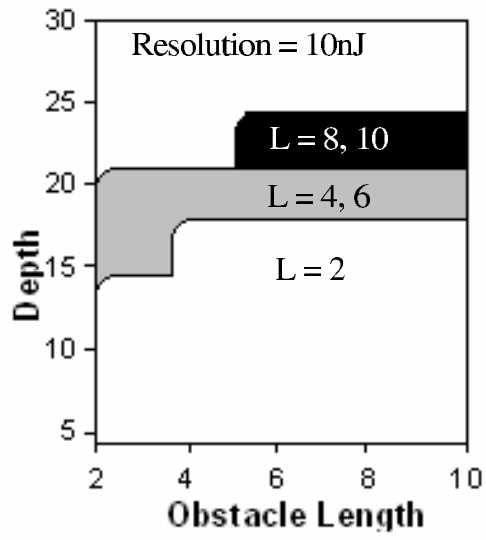
(b)



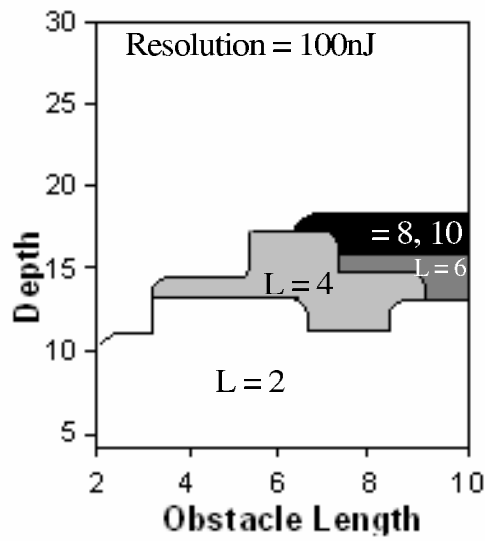
(a)



(b)



(a)



(b)